Progress In Electromagnetics Research Letters, Vol. 105, 17–25, 2022

A Dual-Band Compact Four-Port MIMO Antenna Based on EBG and CSRR for Sub-6 GHz Applications

Yufa Sun[1], Tao Pan[1], Qing Wang[2, *], and Fei Huang[3]

Abstract—A compact sub-6 GHz multiple-input multiple-output (MIMO) antenna based on a complementary split-ring resonator (CSRR) and electromagnetic bandgap (EBG) is proposed in this paper. The antenna has an interesting structure and a compact size of $38 \times 38\,\text{mm}^2$. Four identical antenna elements are deposited orthogonally to each other, using polarization diversity and adding decoupling structures, so that good isolation and miniaturized size can be obtained. The isolation is less than −17.5 dB in the operating bandwidth of 3.28–3.62 GHz and −19.5 dB in 4.78–5.04 GHz. The simulation results are consistent with the measured ones, indicating that the antenna is suitable for Sub-6 GHz communication equipment.

1. INTRODUCTION

With the tremendous increase in mobile communication data throughput, multiple-input multiple-output (MIMO) wireless communication technology has become the core technology of the 5G communication era by virtue of its advantages in multiplying the transmission rate and improving the signal transmission quality without increasing the bandwidth. As for MIMO antenna technology, the research focus is on how to increase the number of antenna elements and make the isolation better between elements as much as possible while ensuring the radiation performance of the antenna in a limited space and meeting the requirements of multiple frequency bands [1].

The coupling between MIMO antennas mainly comes from two aspects. On the one hand, the coupling is from space. This is mainly caused by the antenna's near-field radiation, which causes the mutual influence among the antenna elements. This part of the coupled energy will cause the leakage of the antenna energy. How to minimize this part of the energy and make it radiate into space has become the research focus. On the other hand, it is the coupling from the ground. The energy of the feeder port is mainly coupled to the other end of the antenna element through the ground, which causes an impact. A compact two-dimensional metamaterial structure is proposed in [2] for millimeter wave applications. Based on the characteristic that the equivalent permittivity and equivalent permeability are both negative, the structure is designed to simultaneously enhance isolation and the overall system performance of the MIMO antenna. Reference [3] introduces a new decoupling network structure named dual-band coupled-resonator decoupling network, which improves isolation by about 10 dB. By combining the ground stubs on the bottom layer and the EBG [4] structure on the top layer, the mutual coupling between the radiating patches can be very low. The above three methods belong to spatial decoupling. Ground decoupling is as follows. The defected ground structure (DGS) with specific shape has a significant impact on antenna performance. High isolation is achieved with a mirrored F-shaped DGS which is accordingly improved from around 10 dB to 25 dB [5]. In [6], by introducing

Received 26 April 2022, Accepted 6 June 2022, Scheduled 12 July 2022

* Corresponding author: Qing Wang (xiaoqing5921@126.com).

[1] Key Lab of Intelligent Computing & Signal Processing, Ministry of Education, Anhui University, Hefei 230601, China. [2] School of Electronic Engineering, Anhui Xinhua University, Hefei 230000, China. [3] School of Mechanical and Electronics Engineering, Suzhou University, Suzhou 234000, China.

rectangular metal parasitic radiation patches, the isolation of the dual-polarized antenna is improved by 8 dB. Complementary split-ring resonator (CSRR) can represent an LC circuit resonator because it can store low-frequency energy and "trap" ground currents, inhibiting currents from reaching other components [7]. These CSRR characteristics significantly improve antenna isolation by preventing most of the current from flowing between the two antennas. CSRR can also improve impedance matching, which contributes two operating modes at 3.4 GHz and 3.9 GHz in [8]. In addition to the decoupling structures listed above, more classic decoupling methods include neutral line decoupling, floor branch decoupling, parasitic unit decoupling, etc. For the EBG structure, DGS structure, and floor stubs, some of them can be equivalent to a resonant structure that resonates at the working frequency of the antenna, thereby suppressing the near-field coupling of the antenna or preventing the current at the feeder end from flowing through the floor to another.

This paper proposes a compact four-port MIMO antenna based on five vias mushroom-type EBG and L-shaped complementary split-ring resonators (CSRRs). L-shaped CSRRs are deposited in the ground for enhancing return loss. Moreover, the mushroom-type EBG of five vias has improved isolation which is better than the traditional one via mushroom-type EBG. The antenna consists of a feeder line etched into the top face of the dielectric substrate, an L-shaped radiating patch with seven rounds, and a stair-shaped radiating patch connected to the feeder line which is just above the CSRRs. The four identical antenna units are deposited orthogonally to each other for better isolation. The measurement results illustrate that the antenna operating frequency bands are 3.28–3.62 GHz and 4.78–5.04 GHz.

2. ANTENNA DESIGN

2.1. Design Procedures

As shown in Fig. 1, antenna 1 is an initial model. Each unit of antenna 1 consists of an L-shaped radiating patch with 7 rounds and a stepped radiating patch. L-shaped CSRRs are added on the ground to form antenna 2 for improving the return loss. The simulated S_{11} results are displayed in Fig. 2 to show the effect of the CSRRs. To improve the isolation, antenna 3 is formed by embedding a mushroom-type EBG with one via in the center of antenna 2. Antenna 4 is an improved model of antenna 3 by adding four vias to the four corners of the EBG for further improving the isolation. The simulated S-parameters are shown in Fig. 3, which indicates that the mushroom-type EBG of one via in antenna 3 improves the S_{12} of higher frequency band, while five vias mushroom-type EBG in antenna 4 improves the S_{12} and S_{13} of lower one compared with antenna 2.

2.2. Basic Structure Analysis

On the one hand, CSRR is a ubiquitous meta-structure widely used for adjusting the impedance parameters of the metal patch for better matching. On the other hand, when the CSRR is excited, there is a capacitive effect on the external and internal metal of the structure, and at the same time, there will be an inductive coupling effect between the two structures, resulting in an obvious electrical resonance effect and an electromagnetic stopband [9]. In order to further ameliorate impedance matching, a new L-shaped structure of CSRR is introduced in the ground plane to contribute to the radiation in antenna 2 by guiding surface wave propagation. These CSRRs are placed directly below the antenna radiation patch and orthogonally laid around the ground. From the results in Fig. 2, when the CSRR structure is introduced, the impedance matching of antenna 2 basically meets the requirements. The needed frequency bands can be achieved by modifying the dimensions of the CSRRs. The size of CSRR is corresponding to the center frequency f_i. The total circumference L_i of the CSRR is determined by

$$L_i \approx \frac{c}{2f_i\sqrt{\varepsilon_{eff}}}, \quad \varepsilon_{eff} = \frac{\varepsilon_r + 1}{2}, \quad i = 1, 2 \tag{1}$$

where ε_{eff} is the equivalent permittivity. Through formula (1), the initial values of the circumference L_i of the two split rings can be calculated, and the final value can be obtained through optimization by HFSS.

The EBG structure refers to a periodic artificial magnetic conductor structure with surface wave bandgap characteristics and in-phase reflection characteristics, which is formed by periodically extending

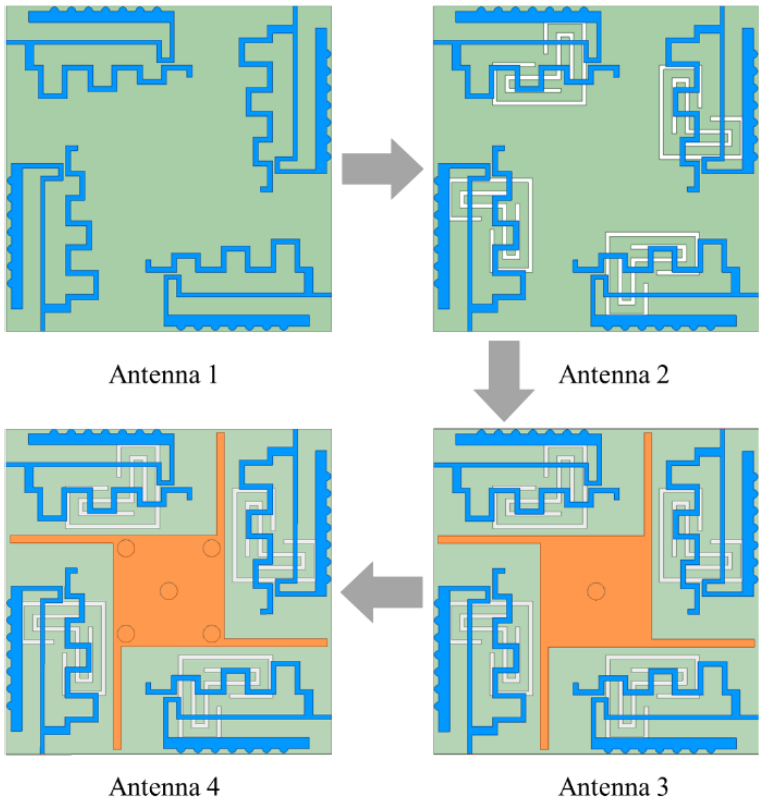

Figure 1. Design of the MIMO antenna.

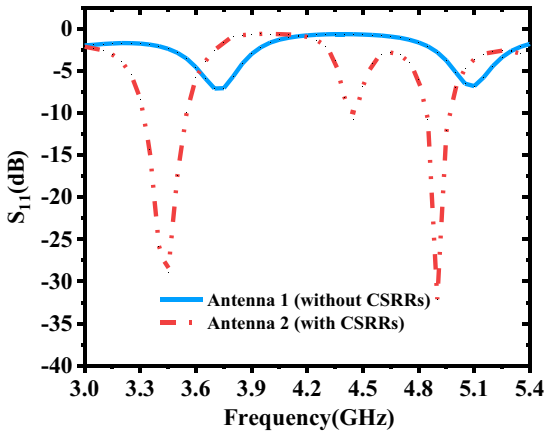

Figure 2. Simulated S_{11} of antenna 1 and 2.

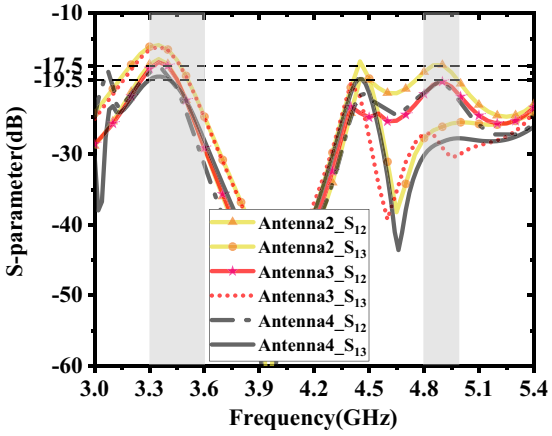

Figure 3. Simulated S-parameters of antenna 2, 3, and 4.

a basic unit into several units [10]. The EBG uses its stopband characteristics to suppress the current from the excitation port to other ports, that is, decreasing the mutual coupling among MIMO antenna elements by suppressing the propagation of surface waves [11]. Therefore, to further weaken the degree of coupling of the antenna elements, EBG is introduced to inhibit surface-wave propagation in antenna 3. As shown in Fig. 4, the innovation of this work is that the mushroom-shaped EBG uses a five-via model instead of a traditional one-via, and four straight parasitic stubs are added around the EBG to increase the isolation between adjacent antenna elements. Since the metal vias mainly play the role of

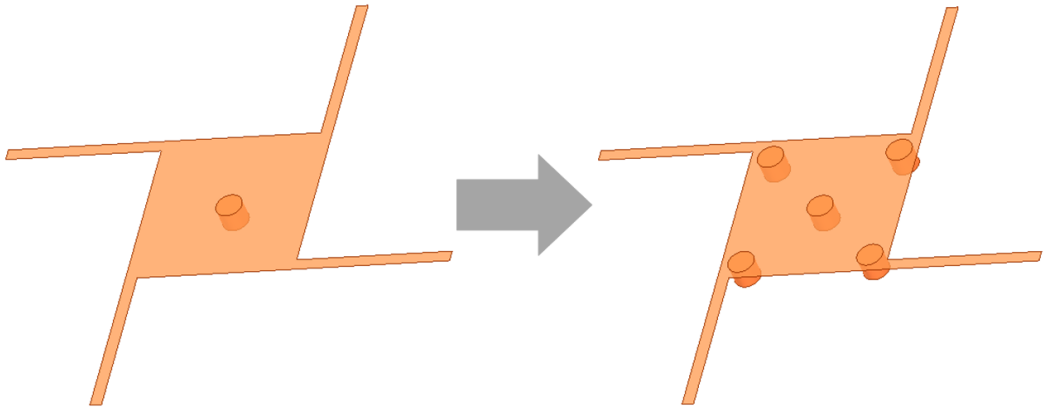

Figure 4. Transformation of the mushroom-shaped EBG. (a) One via. (b) Five vias.

equivalent inductance in the topological circuit, such a design can increase the number of series and parallel inductances in the equivalent circuit, which has a good effect on inhibiting electromagnetic waves. After adding four vias, the isolation S_{13} of antenna 4 at low frequency band is reduced by 4 dB compared with antenna 3, and S_{12} is reduced by 0.8 dB, while in 4.8–5.0 GHz, S_{13} is reduced by 0.7 dB, and S_{12} is basically unchanged.

2.3. The Antenna Configuration

In Fig. 5, the actual size and geometry of the designed MIMO antenna are given, and its total size is 38 mm × 38 mm. The antenna is devised on a 1.6 mm-thick FR-4 substrate whose relative permittivity is 4.4, and loss tangent is 0.02. Four elements are placed in an orthogonal manner which are etched on the FR-4 substrate so that the coupling between port 1 and port 2, and port 1 and port 4 can be reduced by the way of polarization diversity. The surface current distribution in Fig. 6(a) shows that the current is mainly concentrated on the L-shaped radiating patch at 3.45 GHz. In Fig. 6(b), the current is mainly focused on the stepped radiation patch at 4.90 GHz. The dimensional details of the proposed antenna are optimized by HFSS 17.2 in the electromagnetic simulation software ANSYS, as shown in Table 1. The numerical simulation environment of HFSS is that the incident voltage at excitation port of the antenna is 1 V; the port type is lumped port; and the size of radiation box is $120 \times 120 \times 80\,\text{mm}^3$.

Table 1. Dimensions of the proposed antenna.

Parameters	**X1**	**X2**	**X3**	**X4**	**X5**	**X6**	**X7**	**X8**	**X9**
Value (mm)	**0.5**	**3.0**	**3.3**	**2.475**	**1.7**	**1.425**	**4.0**	**1.3**	**6.0**
Parameters	**Y1**	**Y2**	**Y3**	**Y4**	**Y5**	**Y6**	**Y7**	**Y8**	**Y9**
Value (mm)	**18.1**	**1.0**	**0.6**	**2.4**	**2.2**	**0.5**	**2.0**	**1.0**	**16.5**
Parameters	**E1**	**E2**	**E3**	**E4**	**R1**	**R2**	**G1**	**G2**	**G3**
Value (mm)	**0.9**	**8.4**	**13.0**	**12.0**	**1.0**	**2.0**	**5.0**	**1.5**	**0.5**
Parameters	**G4**	**G5**	**G6**	**G7**	**G8**	**G9**	**G10**	**G11**	**G12**
Value (mm)	**4.0**	**0.5**	**5.5**	**10.0**	**6.9**	**11.0**	**6.5**	**5.0**	**5.0**

3. RESULTS AND DISCUSSION

In order to further explore the deviation between the measured results and simulation results of the proposed antenna, and highlight its practicability and reliability, the proposed antenna was fabricated

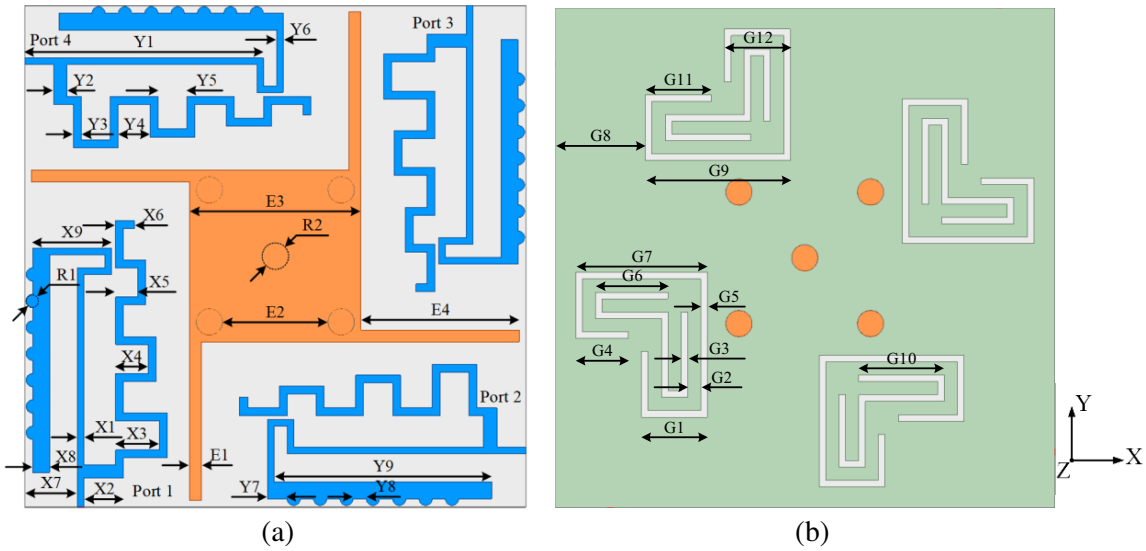

Figure 5. The geometry of the proposed antenna. (a) Top view. (b) Bottom view.

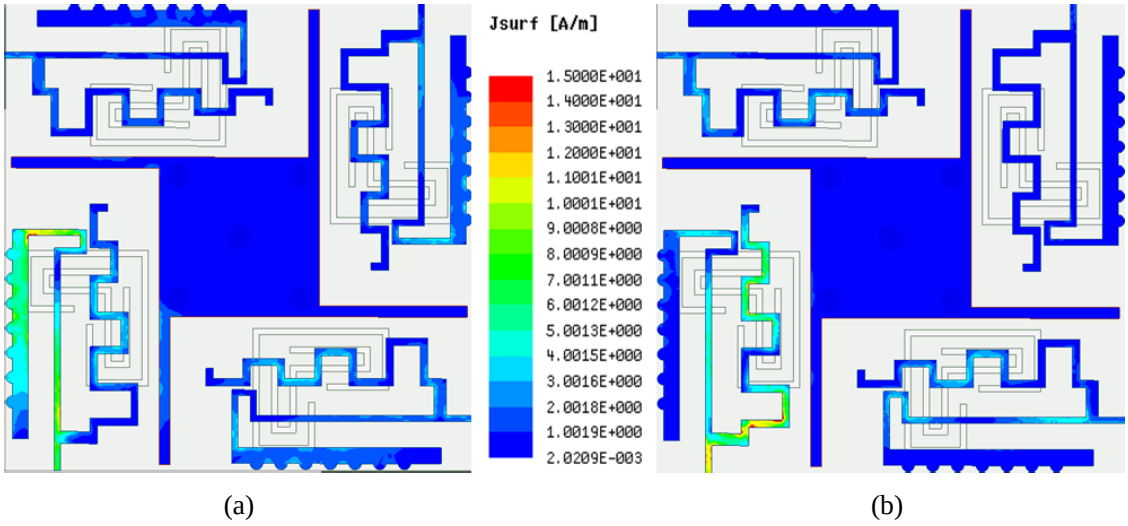

Figure 6. Surface current distributions of the proposed antenna. (a) 3.45 GHz. (b) 4.90 GHz.

according to the dimensions shown in Table 1. Fig. 7(a) shows a photograph of the fabricated MIMO antenna. The antenna S-parameters are measured by using a vector network analyzer. The radiation pattern and gain of the antenna are tested in an anechoic chamber. The measurement setup in the anechoic chamber is as shown in Fig. 7(b), in which the fabricated antenna is at the same height as the standard horn antenna.

3.1. *S*-Parameter

Figure 8 shows the simulated and measured S_{11} parameters of the fabricated antenna. Although there are deviations between the test and simulation results, they can be acceptable. The reason for the deviations is that the port structure after the welding of the SMA connector is not consistent with the simulated ideal port. In addition, there will be a certain deviation between the actual antenna and the design drawing, which will cause the resonant frequency deviation. Simulated and measured isolations

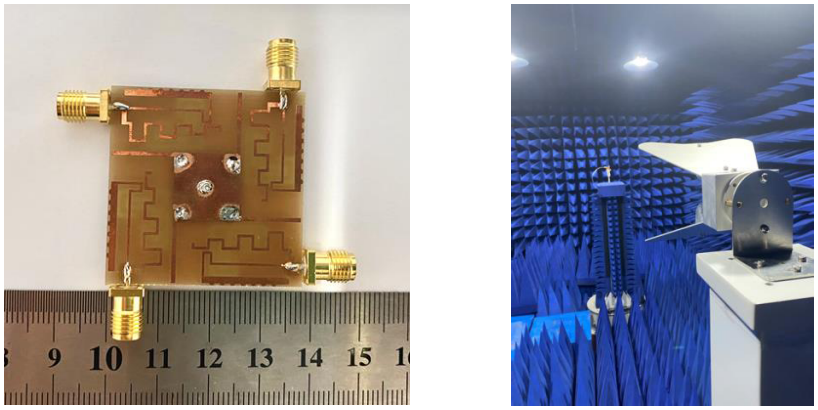

Figure 7. (a) Photograph of the fabricated antenna and (b) measurement setup in anechoic chamber.

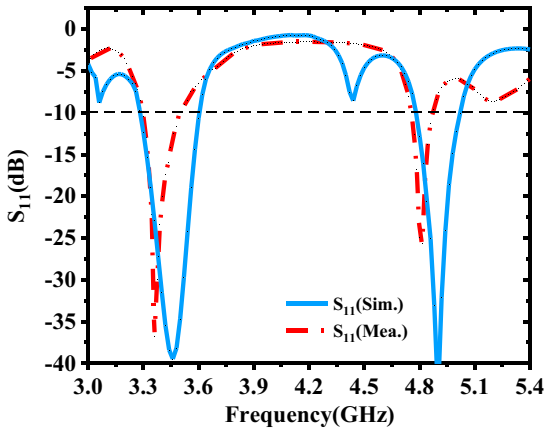

Figure 8. Simulated and measured S_{11}.

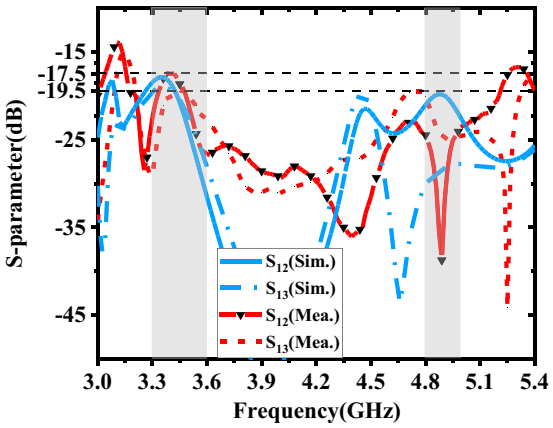

Figure 9. Simulated and measured isolation.

are shown in Fig. 9. It can be seen that the measured isolation between the antenna elements is less than −17.5 dB in the lower frequency band and −19.5 dB in the higher frequency band.

3.2. Radiation Pattern and Gain

Figure 10 shows the measured and simulated 2D radiation patterns of the MIMO antenna. Two frequency points are selected: 3.45 GHz and 4.9 GHz, which are exactly the center points of the two frequency bands of Sub-6 GHz. The radiation patterns are measured when a single target antenna element is excited, and the other three elements are impedance matched by terminating a 50 Ω load. In the figures, the simulation results are basically consistent with the measurement ones.

The simulated and measured gains of the fabricated MIMO antenna are shown in Fig. 11. The gain of the antenna is relatively stable in the Sub-6 GHz frequency band, and the simulated value has little error with the measured one. The simulated value is concentrated from 3.1 to 4.5 dBi, while the measured one is concentrated from 2 to 3.4 dBi, indicating that the antenna do not have bad gain characteristics.

3.3. Diversity Analysis

Envelope Correlation Coefficient (ECC) is one of the most significant parameters in MIMO antenna systems. ECC represents the correlation between the received and transmitted signals between the

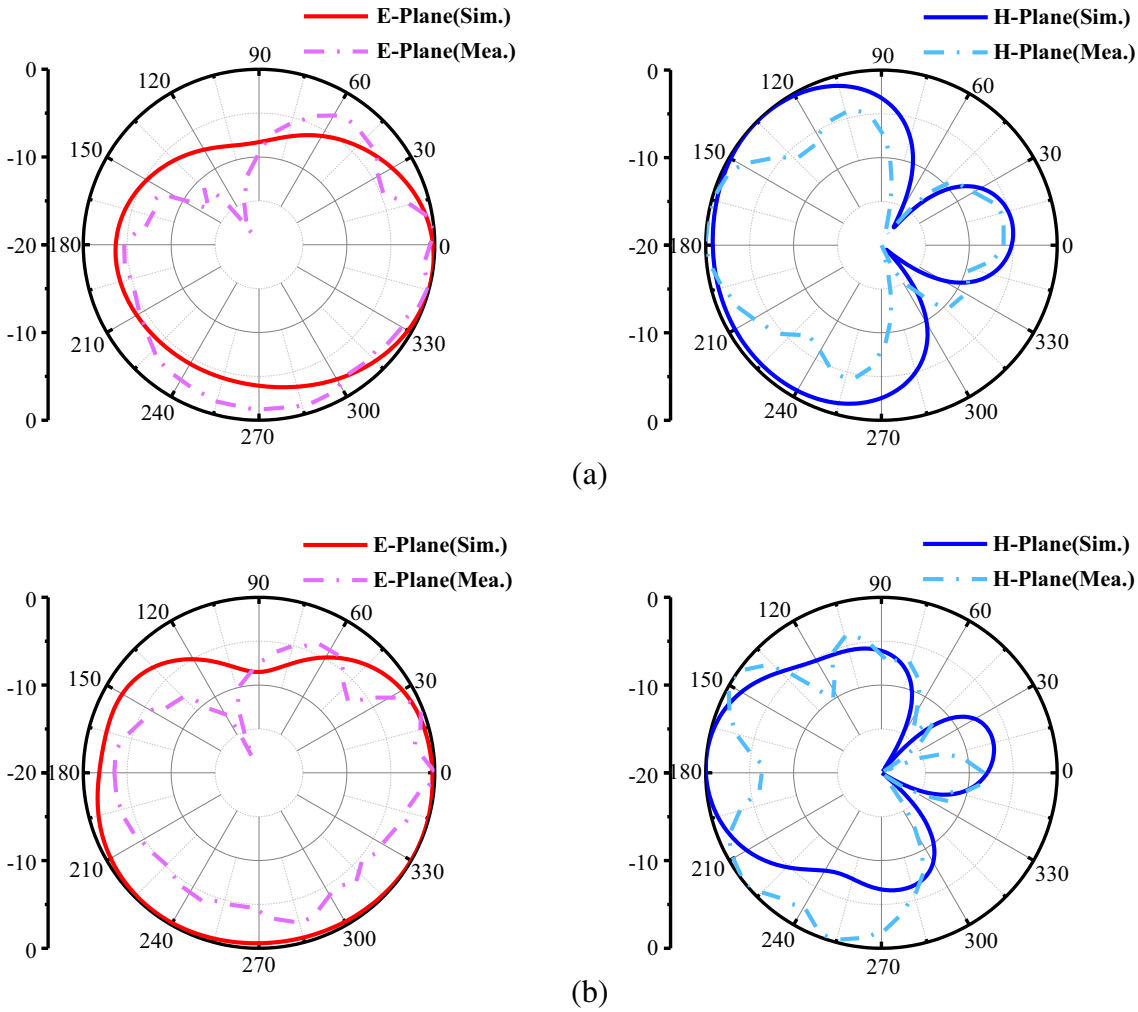

Figure 10. Simulated and measured radiation patterns at (a) 3.45 GHz and (b) 4.9 GHz.

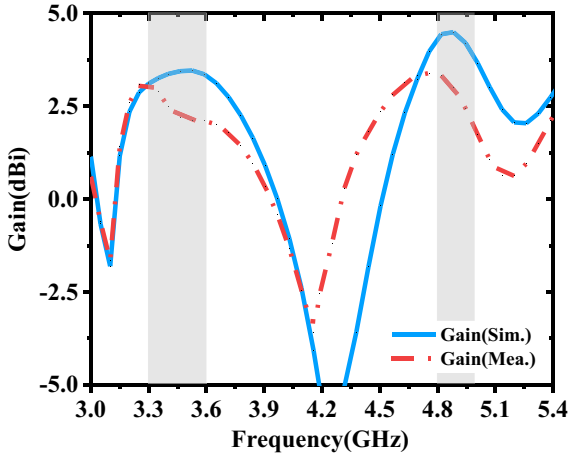

Figure 11. Simulated and measured gains.

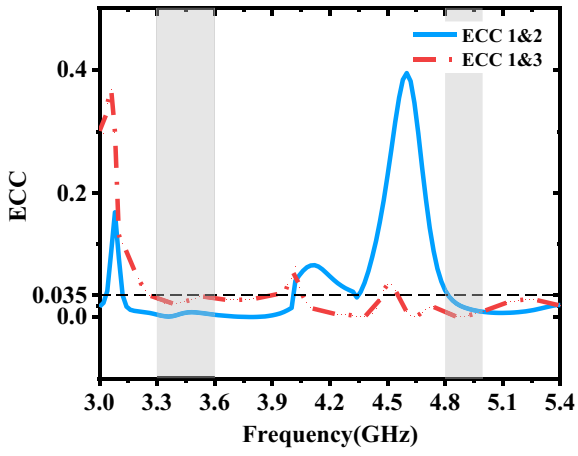

Figure 12. ECC of the MIMO antenna.

antenna elements and can be used to evaluate the diversity characteristics of the antenna. In general, a high value of ECC indicates low diversity characteristics of the antenna. For an N-element MIMO antenna, the ECC can be calculated by Equation (2), where the antenna elements are denoted by i, j.

$$\mathrm{ECC} = \frac{\left|S_{ii}^{*}S_{ij} + S_{ji}^{*}S_{jj}\right|^{2}}{\left|1 - |S_{ii}|^{2} - |S_{ji}|^{2}\right|\left|1 - |S_{jj}|^{2} - |S_{ij}|^{2}\right|}. \tag{2}$$

The results of ECC are shown in Fig. 12. The calculated ECC of the antenna in both frequency bands is less than 0.035, which is far less than the engineering value of 0.5, indicating that the MIMO antenna has good diversity and isolation characteristics.

Finally, as shown in Table 2, the antenna in this paper is compared with the antennas in [12–18]. Although some antennas have higher isolation, they are larger in size; some antennas are small in size, but the ECC or gain is not good enough. To sum up, the antenna in this paper has an excellent isolation effect on the basis of realizing the miniaturized design.

Table 2. Performance comparison with previous literature.

References	Antenna size (mm × mm)	Bandwidth (GHz)	Isolation (dB)	Gain (dBi)	ECC
[12]	70 × 70	4.4–5.7	16	2.0	< 0.007
[13]	41 × 41	3.47–3.53, 5.68–5.72	18.4, 22.7	2.9	< 0.08
[14]	45 × 45	2–10.6	17	4.6	< 0.005
[15]	60 × 60	2.54–3.2	15	3.2	< 0.02
[16]	38.3 × 38.3	3–13.2	17	6.3	< 0.02
[17]	40 × 40	3–11	15	2.7	NA
[18]	60 × 60	3.4–3.8	19	4.5	< 0.12
this work	**38 × 38**	**3.28–3.62, 4.78–5.04**	**17.5, 19.5**	**3.4**	**< 0.035**

4. CONCLUSION

A four-element MIMO antenna is proposed in this paper which can cover the sub-6 GHz frequency band. The antenna has a compact size of 38 mm × 38 mm, which uses L-shaped CSRRs to enhance impedance matching and mushroom-shaped EBG to reduce sub-6G dual-band coupling. The isolation is better than −17.5 dB and −19.5 dB over the lower and higher frequency bands. The fabricated MIMO antenna achieves satisfactory diversity performance in terms of isolation and ECC. It has broad application prospect in sub-6 GHz MIMO antenna. However, SMA connectors need to be designed in the simulation process, and attention should be paid to the fabricated precision of the antenna.

ACKNOWLEDGMENT

This work was partially supported by the National Natural Science Foundation of China Project 62071004 and the Anhui Local High-level University Construction Project 2013gx001.

REFERENCES

1. Andrews, J. G., et al., "What will 5G be?" *IEEE Journal on Selected Areas in Communications*, Vol. 32, No. 6, 1065–1082, Jun. 2014.
2. Al-Bawri, S. S., M. T. Islam, T. Shabbir, G. Muhammad, M. S. Islam, and H. Y. Wong, "Hexagonal shaped near zero index (NZI) metamaterial based MIMO antenna for millimeter-wave application," *IEEE Access*, Vol. 8, 181003–181013, 2020.

3. Zhao, L. and K. Wu, "A dual-band coupled resonator decoupling network for two coupled antennas," *IEEE Transactions on Antennas and Propagat.*, Vol. 63, No. 7, 2843–2850, Jul. 2015.
4. Khan, A., S. Bashir, S. Ghafoor, and K. K. Qureshi, "Mutual coupling reduction using ground stub and EBG in a compact wideband MIMO-antenna," *IEEE Access*, Vol. 9, 40972–40979, 2021.
5. Jamal, M. Y., M. Li, and K. L. Yeung, "Isolation enhancement of closely packed dual circularly polarized MIMO antenna using hybrid technique," *IEEE Access*, Vol. 8, 11241–11247, 2020.
6. Yin, B., S. Zhao, P. Wang, and X. Feng, "Isolation improvement of compact microbase station antenna based on metasurface spatial filtering," *IEEE Transactions on Electromagnetic Compatibility*, Vol. 63, No. 1, 57–65, Feb. 2021.
7. Khan, M. S., A. Capobianco, S. M. Asif, D. E. Anagnostou, R. M. Shubair, and B. D. Braaten, "A compact CSRR-enabled UWB diversity antenna," *IEEE Antennas and Wireless Propagat.*, Vol. 16, 808–812, 2017.
8. Dash, J. C. and D. Sarkar, "A four-port CSRR-loaded dual-band MIMO antenna with suppressed higher order modes," *IEEE Access*, Vol. 10, 30770–30778, 2022.
9. Ren, Y., K. Li, F. Wang, B. Gao, and H. Wu, "A broadband magnetic coupling microstrip to waveguide transition using complementary split ring resonators," *IEEE Access*, Vol. 7, 17347–17353, 2019.
10. Abbas, A., N. Hussain, J. Lee, S. G. Park, and N. Kim, "Triple rectangular notch UWB antenna using EBG and SRR," *IEEE Access*, Vol. 9, 2508–2515, 2021.
11. Al-Hasan, M. J., T. A. Denidni, and A. R. Sebak, "Millimeter-wave compact EBG structure for mutual coupling reduction applications," *IEEE Transactions on Antennas and Propagat.*, Vol. 63, No. 2, 823–828, Feb. 2015.
12. Deng, H., T. Xu, Y. Xue, F. Liu, and L. Sun, "Closely spaced broadband MIMO differential filtering slotline antenna with CM suppression," *IEEE Antennas and Wireless Propagat.*, Vol. 17, No. 12, 2498–2502, Dec. 2018.
13. Boukarkar, A., X. Q. Lin, Y. Jiang, L. Y. Nie, P. Mei, and Y. Q. Yu, "A miniaturized extremely close-spaced four-element dual-band MIMO antenna system with polarization and pattern diversity," *IEEE Antennas and Wireless Propagat.*, Vol. 17, No. 1, 134–137, Jan. 2018.
14. Tripathi, S., A. Mohan, and S. Yadav, "A compact Koch fractal UWB MIMO antenna with WLAN band-rejection," *IEEE Antennas and Wireless Propagat.*, Vol. 14, 1565–1568, 2015.
15. Jiang, W., Y. Liu, Y. Cui, B. Wang, and S. Gong, "Compact wide-band MIMO antenna with high port isolation," *12th European Conference on Antennas and Propagat.*, 1–3, 2018.
16. Gómez-Villanueva, R. and H. Jardón-Aguilar, "Compact UWB uniplanar four-port MIMO antenna array with rejecting band," *IEEE Antennas and Wireless Propagat.*, Vol. 18, No. 12, 2543–2547, Dec. 2019.
17. Mao, C. and Q. Chu, "Compact coradiator UWB-MIMO antenna with dual polarization," *IEEE Transactions on Antennas and Propagat.*, Vol. 62, No. 9, 4474–4480, Sept. 2014.
18. Saxena, S., B. K. Kanaujia, S. Dwari, S. Kumar, H. C. Choi, and K. W. Kim, "Planar four-port dual circularly-polarized MIMO antenna for sub-6 GHz band," *IEEE Access*, Vol. 8, 90779–90791, 2020.